Azacyanocarbon chemistry. Comparison of the hexacyano-3,4-diazahexa-1,5-dienediide $[C_{10}N_8]^{2-}$ with the corresponding radical anion $[C_{10}N_8]^{\cdot -}$: electrochemical and EPR studies, crystallographic and electronic structures

Marc Decoster,[a] Françoise Conan,[a] Marek Kubicki,†[,b] Yves Le Mest,[a] Philippe Richard,[b] Jean Sala Pala*[,a] and Loïc Toupet[c]

[a] *Laboratoire de Chimie, Electrochimie Moléculaires et Chimie Analytique, URA CNRS 322, Université de Bretagne Occidentale, Faculté des Sciences, 29285 Brest-Cedex, France*
[b] *Université de Bourgogne, BP 134, 21000 Dijon Cedex, France*
[c] *Groupe Matière Condensée et Matériaux, URA CNRS 804, Université de Rennes I, Faculté des Sciences, 35042 Rennes-Cedex, France*

Electrochemical, spectrochemical and structural characterization of the tetraalkylammonium salts of the 1,1,2,5,6,6-hexacyano-3,4-diazahexa-1,5-dienediide anion $[(R_4N)_2(C_{10}N_8)$: R = Et 1a; R = Bu 1b] are reported. The dianion displays two one-electron reversible oxidation processes at $E'^0_1 = -0.10$ V $[(C_{10}N_8)^{\cdot -}/(C_{10}N_8)^{2-}]$ and $E'^0_2 = +0.59$ V $[(C_{10}N_8)/(C_{10}N_8)^{\cdot -}]$ (ref. Fc^+/Fc). Solutions of the radical anion have been prepared by bulk electrolysis and fully characterized by EPR spectroscopy. Chemical oxidation of 1a by iodine in dichloromethane affords this radical anion as its tetraethylammonium salt $(Et_4N)(C_{10}N_8)$ 3a. $(C_{10}N_8)^{2-}$ and $(C_{10}N_8)^{\cdot -}$ have unequivocally different IR and visible spectra. Single crystal X-ray diffraction studies of 1b and 3a have been carried out. In 1b, the dianion is planar within ±0.03 Å and has a crystallographically imposed $\bar{1}$ symmetry but the point group is approximately C_{2h} while in 3a the $(C_{10}N_8)^{\cdot -}$ unit, which has no crystallographically imposed symmetry, is only roughly planar. In both cases, the two $-C(CN)C(CN)_2$ groups are in *trans* positions relative to the N–N bond. The crystal structure of 3a clearly shows that the anion exist as dimer units $[(C_{10}N_8)_2]^{2-}$. This is in agreement with the EPR spectra and the molecular orbital study carried out at the semi-empirical AM1 level which both indicate a thermally populated triplet excited state.

Neutral and anionic cyanocarbons and azacyanocarbons, defined respectively as polycyanosubstituted moieties with all-carbon and all-carbon and nitrogen backbones and no hydrogen, are interesting synthetic targets.[1,2] Many of their derivatives show interesting optical, electrical and/or magnetic properties.[1–6] Some of them have also been used as dyes and pigments.[7,8] Although a great deal of chemistry has been reported in the literature on cyanocarbanions, even excluding $TCNQ^{\cdot -}$, $TCNE^{\cdot -}$ and $DDQ^{\cdot -}$ (TCNQ = tetracyanoquinodimethane; TCNE = tetracyanoethylene; DDQ = dichlorodicyanobenzoquinone), there were few references[9–11] to the $(C_{10}N_7)^-$ and $(C_{10}N_8)^{2-}$ azacyanocarbanions (Scheme 1) since their syntheses by Middleton *et al.*[12] Therefore, in order to obtain a more unified view of the bonding mode–electronic structure relationship in these and other conjugated anionic systems which might lead to a rationale of their properties of interest, we decided to study the properties of such anions by themselves and as ligands in metal complexes.[13] The objectives of the work described here were (*i*) to fully characterise the $(C_{10}N_8)^{2-}$ closed-shell dianion, (*ii*) to study the possibility of generating the corresponding radical monoanion $C_{10}N_8^{\cdot -}$, and (*iii*) to compare the molecular and electronic structures of these two anionic species.

Results and discussion

Syntheses and solution studies

In agreement with a previous work,[12] TCNE reacted with hydrazine to afford the hexacyanodiazahexadienediide anion which was isolated as tetraalkylammonium salts $(R_4N)_2(C_{10}N_8)$ (**1a** R = Et; **1b** R = Bu). During the synthesis of **1a**, obtention of a minor derivative **2a** was observed for which elemental analyses, ^1H and ^{13}C NMR data are consistent with the formulation $(Et_4N)_2[(NC)_2CC(CN)NNC(CN)C(CN)(NHNH_2)]\cdot 1.5\,H_2O$. **2a** is a slightly hydroscopic orange–red solid. As shown in Fig. 1, $(Et_4N)_2(C_{10}N_8)$ **1a** displays two redox processes in the electrochemical range of benzonitrile. These two oxidation processes $[C_{10}N_8^{\cdot -}/C_{10}N_8^{2-}$: $E'^\circ_1 = -0.10$ V; $C_{10}N_8/C_{10}N_8^{\cdot -}$: $E'^\circ_2 = +0.59$ V (ref. Fc^+/Fc)‡] have cyclic voltammetry (CV)

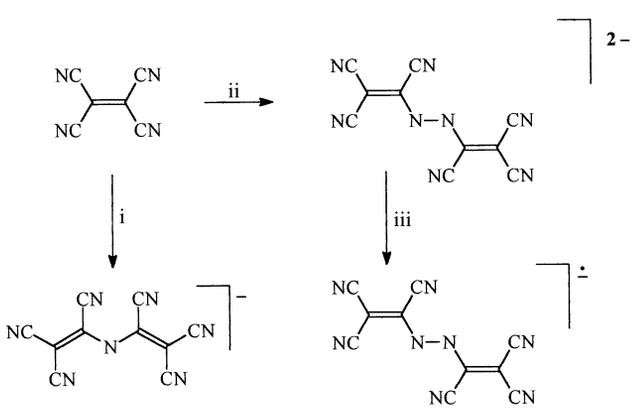

Scheme 1 Syntheses of the $C_{10}N_7^-$, $C_{10}N_8^{2-}$ and $C_{10}N_8^{\cdot -}$ azacyanocarbanions: (*i*) NH_3 in dry acetone;[12] (*ii*) NH_2NH_2, H_2O in water;[12] (*iii*) I_2 in CH_2Cl_2 (this work)

† Laboratoire de Synthèse et d'Electrosynthèse Organométalliques, UMR CNRS 5632.

‡ Throughout this work, the reference electrode used is Fc^+/Fc. For comparison of the present results with other work, the Fc^+/Fc formal potential has been measured *versus* the standard calomel electrode (SCE) in benzonitrile (0.2 M Bu_4NPF_6): $E'^\circ(Fc^+/Fc) = +0.43$ V *vs.* SCE.

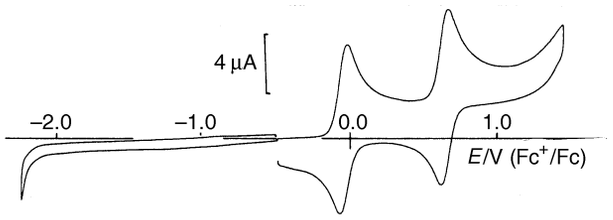

Fig. 1 CV of **1a** $(Et_4N)_2(C_{10}N_8)$ (*ca.* 10^{-3} in PhCN; 0.2 M Bu_4NPF_6; Pt electrode; scan rate 0.1 V s^{-1}; V *vs.* Fc^+/Fc)

characteristics indicative of one electron diffusion-controlled reversible exchanges for scan rate v, $0.1 < v < 1.0$ V s^{-1} (*i.e.* ΔE_p *ca.* 60 mV, i_{pa}/i_{pc} *ca.* constant, $i_p/v^{\frac{1}{2}}$ constant).

Bulk electrolysis of the yellow solution of **1a** at a potential more positive (+0.20 V) than the first reversible oxidation process generates, after an exchange of $n = 1.0 \pm 0.1$ electron per molecule, a brown–red solution. The change of the current intensity with time [$\log i = f(t)$ linear] agrees well with a simple electron exchange as does the CV observed after this electrolysis, which is the same as the initial one except that the first process corresponds now to a reduction. Solutions of the oxidized species are reasonably stable (a few hours). The UV–VIS spectrum of the anion is significantly affected by the oxidation process; the maxima of absorption are shifted from 474 and 454 nm for the starting solution to 506 and 476 nm for the oxidized species solution. At room temperature, the benzonitrile solution of the oxidized species displays a characteristic EPR spectrum centred at g 2.003 (Fig. 2). At a very low modulation a complex hyperfine structure can be clearly seen on the central lines of the spectrum. It is noteworthy that MO calculations reported below allowed us to interpret the observed hyperfine structure arising from coupling with different nitrogen nuclei of the $(C_{10}N_8)^{\bullet -}$ radical taking into account the fact that the coupling constants with the nitrogen nuclear spins should be proportional to the spin densities retained on these atoms. These spin densities may be estimated from the squares of the coefficients affecting the pπ nitrogen atomic orbitals in the HOMO according to the simple McConnell's relation $a_i = Q\ c_i^2$. The corresponding values are gathered in Table 1 (the Q constant is taken as equal to 2.2×10^{-3} T); they lead to a simulated spectrum which presents features similar to that of the experimental spectrum at a high modulation (Fig. 2).

A bulk electrolysis conducted at a potential more positive than the second oxidation process (+0.90 V, exchange of 2.1 ± 0.1 electron per molecule) induces a partial degradation of the solution since a decrease in peak heights is noted on the voltammogram. These results unambiguously establish that the first one-electron oxidation process consists of the generation of the stable radical anion $(C_{10}N_8)^{\bullet -}$ while the second oxidation process generates the instable $(C_{10}N_8)$ species according to eqn. (1).

$$C_{10}N_8^{2-} \underset{e^-}{\overset{E'^\circ_1}{\rightleftharpoons}} C_{10}N_8^{\bullet -} \underset{e^-}{\overset{E'^\circ_2}{\rightleftharpoons}} C_{10}N_8 \qquad (1)$$

Attempts to prepare the oxidized species by chemical oxidation of the dianion were made. Reaction of **1a** with iodine in dichloromethane affords the monoanion as its tetraethylammonium salt $(Et_4N)(C_{10}N_8)$ **3a** in good yield (*ca.* 80%). **3a** and **1a** may be easily distinguished by their IR and VIS spectra (see Experimental part). Furthermore, in benzonitrile, **1a** gives no EPR signal while **3a** displays a spectrum similar to that of the electrogenerated species.

By comparison with the work on tetracyano-1,4-benzoquinone, *Q*, which is to date the strongest acceptor that has been isolated in the neutral form ($Q/Q^{\bullet -}$: $E'^\circ = 0.52$ V),[14] attempts to obtain $C_{10}N_8$ ($C_{10}N_8/C_{10}N_8^{\bullet -}$: $E'^\circ_2 = +0.59$ V) by bromine or chlorine oxidation of the disilver salt $Ag_2C_{10}N_8$[12] were made. Colour change and precipitation of silver halide were observed but we were unable to isolate the dioxidized neutral species.

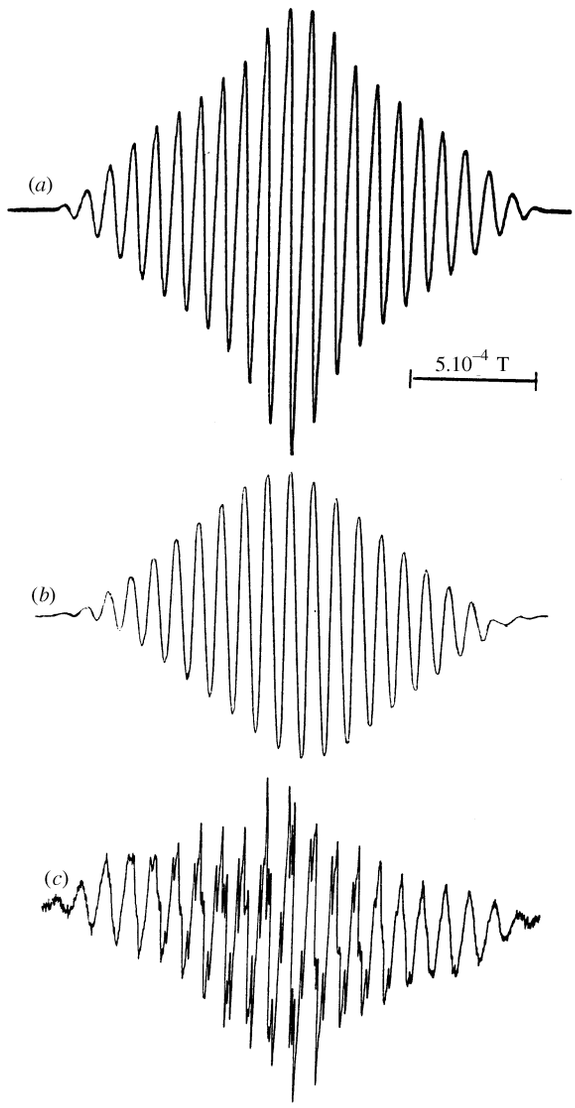

Fig. 2 RT EPR spectra of a benzonitrile solution of **1a** $(Et_4N)_2(C_{10}N_8)$ after electrolysis at a potential more positive (+0.20 V) than the first reversible oxidation process: (*a*) experimental spectrum recorded at a modulation of 6.3×10^{-4} T; (*b*) simulated spectrum obtained with the coupling constants given in Table 1. The signal is centred at g 2.003; (*c*) experimental spectrum partially resolved at a modulation of 0.063×10^{-4} T. This spectrum could not be simulated at this level of resolution owing to limitations of the calculation program.

Table 1 ESR coupling constants a_{exp} and a_{calc} $(= Qc_i^2)$ $(10^{-4}$ T) for the $(C_{10}N_8)^-$ radical. (The labelling scheme for the nitrogen atoms is given in Fig. 6)

	N_1	N_2	N_3	N_4
a_{exp}	2.80	0.16	0.90	0.90
$Q\ ci^2$	2.98	0.19	0.85	0.85

Crystal structures

$(Bu_4N)_2(C_{10}N_8)$ 1b. Compound **1b** crystallizes in the triclinic $P\bar{1}$ space group; the asymmetric unit contains two cations related by an inversion centre and one anion which has crystallographic imposed $\bar{1}$ symmetry. However, the anion, which is planar within ± 0.03 Å, also presents a pseudo twofold axis and

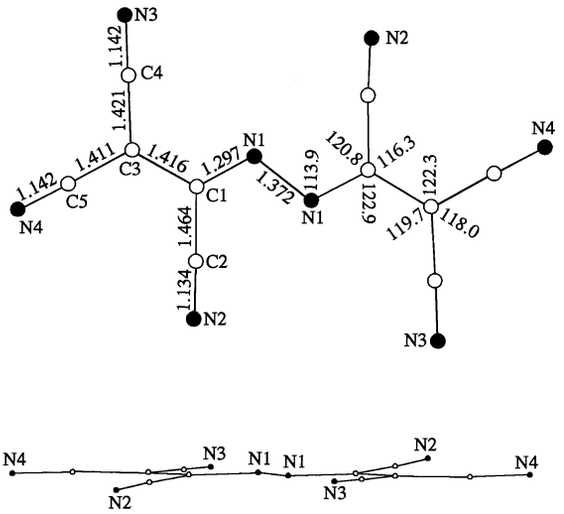

Fig. 3 Two different views of the $(C_{10}N_8)^{2-}$ anion in **1b** $(Bu_4N)_2(C_{10}N_8)$: atom numbering, bond lengths (Å, esd values in least significant digits: 3 or 4) and bond angles (°, esd values in least significant digits: 3)

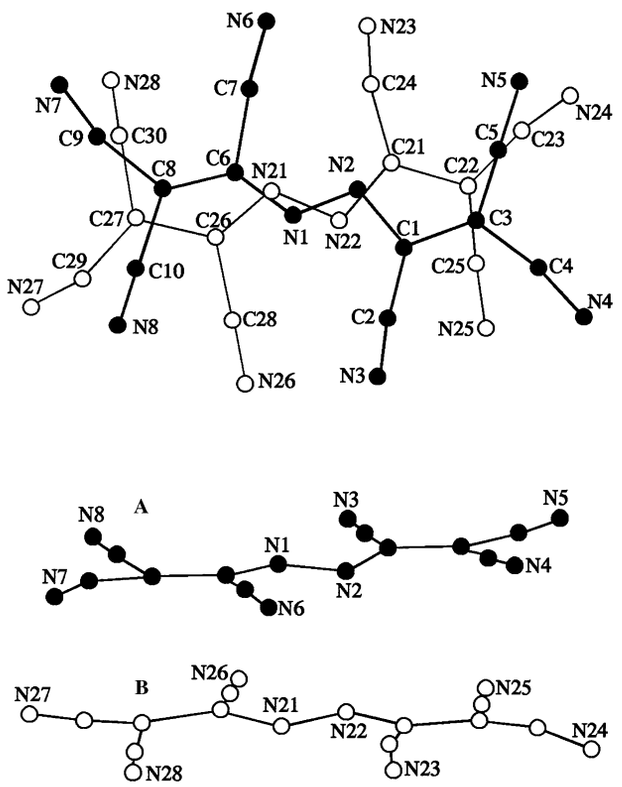

Fig. 4 Two different views of the $[(C_{10}N_8)_2]^{2-}$ anion in **3a** $(Et_4N)(C_{10}N_8)$ with the atom numbering

a pseudo mirror plane and its point group is therefore approximately C_{2h} (Fig. 3).

In the dianion, the two $C(CN)C(CN)_2$ groups are in *trans* positions relative to the N(1)–N(1′) bond. The C(1)–N(1)–N(1′) value [113.9(3)°] argues strongly for a sp^2 and not a sp^3 hybridization of the central N atoms. The N(1)–N(1′) bond length [1.372(4) Å], although shorter than N_a–N_b single bond lengths[15] (*ca.* 1.40 Å with N_a and N_b planar, *ca.* 1.45 Å with N_a and N_b pyramidal), is much longer than that found for *trans*-C–N=N–C units (*ca.* 1.22 Å)[15] indicating only a slight character of multiplicity.

The C(1)–N(1) bond length [1.297(3) Å], shorter than the usual C_{sp^2}–N single bond lengths (1.33 to 1.38 Å with N_{sp^2} planar and up to 1.42 Å for N_{sp^3} pyramidal), may be compared with the 1.273 Å given by Allen *et al.*[15] for C_{sp^2}=N double bonds. The C(1)–C(2) and C(1)–C(3) bond lengths [1.464(4) and 1.416(4) Å, respectively] indicate that electronic delocalization occurs over each $NC(CN)C(CN)_2$ fragment. Bond angle values at the C(1) and C(3) atoms [from 116.3(3) to 122.9(3)°; sum = 360.0° at each atom] are in agreement with a sp^2 hybridization of these carbon atoms (Fig. 3). For the nitrile groups, the C–N bond length is slightly longer for the groups on the 'terminal' C(3) carbon atom [1.142(4) Å for C(4)–N(3) and C(5)–N(4)] than for the C(2)–N(2) groups [1.134(4) Å] bonded to the C(1) atom in α position relative to the N(1) atom; all of them have usual values.

$(Et_4N)(C_{10}N_8)$ 3a. Compound **3a** crystallizes in the monoclinic space group *Cc*; the asymmetric unit consists of two cations and two $C_{10}N_8^{\bullet -}$ anions. However, the anion exists as $[(C_{10}N_8)_2]^{2-}$ dimer units and is therefore composed of two crystallographically different $(C_{10}N_8)^{\bullet -}$ moieties denoted **A** and **B** (Fig. 4).

Although deviations from planarity are more important than for $(C_{10}N_8)^{2-}$ in **1b**, each $(C_{10}N_8)^{\bullet -}$ unit may be considered as roughly planar (maximum of deviation from the mean plane: 0.19 for **A**, 0.18 Å for **B**). As in the dianion, the two $C(CN)C(CN)_2$ groups are in the *trans* positions relative to the N–N bond. Within the dimer, the two mean planes are almost parallel (dihedral angle 2.8°) and the intradimer separation between the mean planes (*ca.* 3.0 Å) is significantly less than the generally accepted 3.4–3.5 Å van der Waals separation. Such dimerization is often observed with roughly planar radicals. As for example, $(TCNQ)^{\bullet -}$ often exists as $[(TCNQ)_2]^{2-}$ dimers which usually exhibit slipped eclipsed configurations where slippage occurs along either the short or the long TCNQ axis.[16–18] In **3a**, the geometry of the $[(C_{10}N_8)_2]^{2-}$ dimer roughly corresponds, starting from the perfectly eclipsed form, to a two-fold rotation of one of the $(C_{10}N_8)^{\bullet -}$ unit about an axis parallel to the N–N bonds.

The character of multiplicity of the central N–N bond [1.25(1) Å in **A**; 1.32(2) Å in **B**] is greater than in the $(C_{10}N_8)^{2-}$ dianion. However, some crystallographic problems encountered in the resolution of the structure of **3a** precluded a sharp comparison of the $(C_{10}N_8)^{-}$ geometry with that of $(C_{10}N_8)^{2-}$: the number of observed reflections was low; high thermal motion and disorder were found for some of the carbon atoms of the cations. This resulted in rather high esd values for bond lengths and bond angles.

Solid state EPR spectra and magnetic susceptibility

Finely divided powder samples of $(Et_4N)(C_{10}N_8)$ **3a** at room temperature and at 150 K have a central line present in the EPR spectra at g 2.003 attributed to radical impurities at low level, most likely $(C_{10}N_8)^{\bullet -}$ (Fig. 5). The features of the left and right of this central line are absorptions characteristic of randomly oriented triplets and can be analysed in terms of the standard spin Hamiltonian containing the electronic Zeeman term and the zero-field splitting (ZFS) term describing the dipolar interaction between the two unpaired electrons.[19–23] The two ZFS parameters, D, which provides a measure of the average distance between the interacting electrons in the triplet, and E, which is sensitive to the asymmetry of the triplet wavefunction and vanishes for wavefunctions with threefold and higher symmetry, were extracted from the triplet-state powder spectra of **3a** using eqns. (2)–(4) where ΔH_z is the separation between

$$\Delta H_z = 2D \quad (2)$$

$$\Delta H_y = D + 3E \quad (3)$$

$$\Delta H_x = D - 3E \quad (4)$$

the outermost pair of absorptions, ΔH_y is the separation between the next pair of absorptions, and ΔH_x is the separation between the innermost pair of signals. At room temperature,

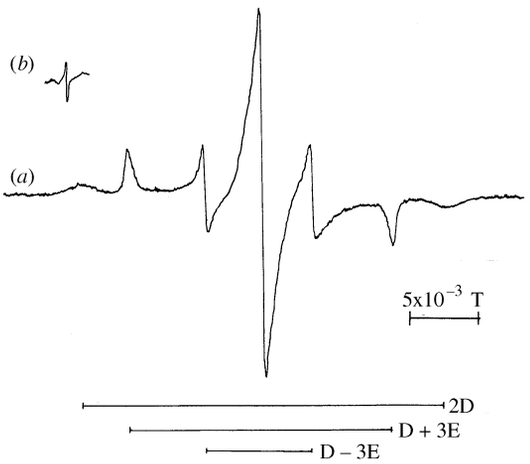

Fig. 5 RT powder ESR spectrum of **3a** $(Et_4N)(C_{10}N_8)$: (*a*) $\Delta m_s = \pm 1$ transitions; (*b*) 'forbidden' half-field $\Delta m_s = \pm 2$ transitions

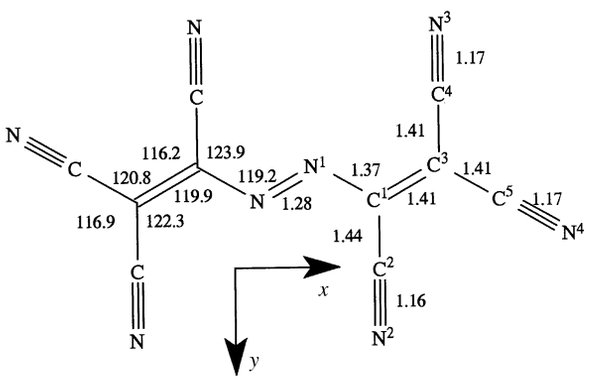

Fig. 6 AM1 optimized structure for $(C_{10}N_8)^{\bullet -}$ radical with bond lengths (Å) and bond angles (°). The axis origin is on the inversion centre of the molecular system.

the values of the *D* and *E* parameters are $|D| = 1.35\ 10^{-2}\ T$ ($|D|/hc = 0.0126\ cm^{-1}$) and $|E| = 2.1\ 10^{-3}\ T$ ($|E|/hc = 0.0020\ cm^{-1}$). This value for *D* is of the same order of magnitude as that found for the $[|C_3\{C(CN)_2\}_3|_2]^{2-}$dimer.[22] The average distance between the two interacting electrons can be estimated from *D* to be *ca.* 6 Å. Further confirmation of the triplet-state is provided by the observation of the 'forbidden' $\Delta m_s = \pm 2$ half-field absorption (Fig. 5). The intensities of the EPR absorptions decrease with decreasing temperature indicating that the triplet state is thermally populated and cannot be the ground state. Compound **3a** exhibits essentially temperature independent diamagnetic behaviour below 270 K with a small paramagnetic contribution attributed to $(C_{10}N_8)^{\bullet -}$ impurities detected by EPR. From room temperature, the magnetic susceptibility increases with increasing temperature; this observation is also in agreement with a thermally populated triplet excited state.

Electronic structures of $(C_{10}N_8)^{\bullet -}$ and $[(C_{10}N_8)_2]^{2-}$

In order to interpret the solution EPR spectrum of the $(C_{10}N_8)^{\bullet -}$, the triplet state observed for the dimer $[(C_{10}N_8)_2]^{2-}$, as well as the optical properties of these two entities, a study of molecular orbital states has been carried out at the semi-empirical AM1 level.[24]

The $(C_{10}N_8)^{\bullet -}$ radical. The molecular structure of the isolated radical not being available (the X-ray determination concerns the diamagnetic dimer form), its geometry has been optimized by using a UHF AM1 semi-empirical hamiltonian. A planar molecule possessing C_{2h} point symmetry was obtained (Fig. 6).

In order to check the validity of this method, a similar optimization has been carried out on the dianion $(C_{10}N_8)^{2-}$ whose crystal structure is known. A very good overall agreement

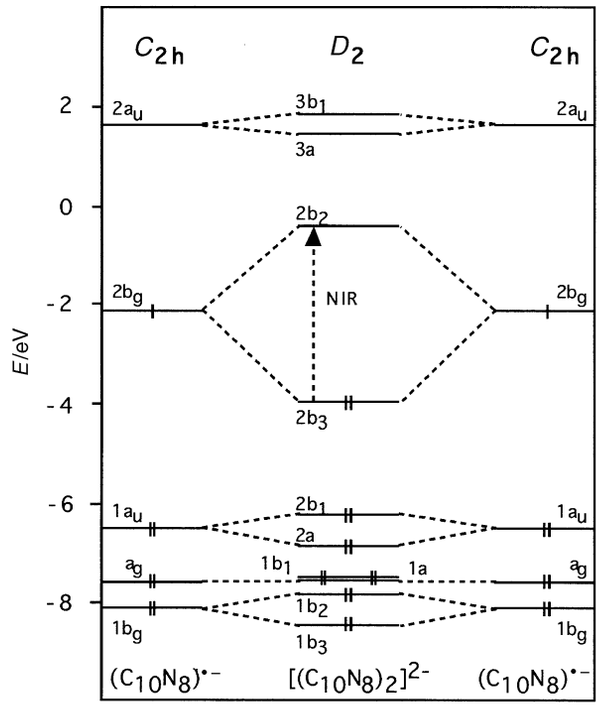

Fig. 7 Partial molecular orbital interaction diagram for $(C_{10}N_8)^{\bullet -}$ and $[(C_{10}N_8)_2]^{2-}$. The electronic transition giving rise to the NIR absorption in the dimer is shown.

between the calculated and the X-ray geometries was observed, with the exception of the N(1)–C(1)–C(2) angle (Fig. 3) which was slightly overestimated in our calculation (124.3° *vs.* 120.8°). Thus, the method used is well adapted for this type of anion, and consequently, the optimized structure of the radical may be submitted to the molecular orbital calculations. The energy levels are shown in Fig. 7. The unpaired electron occupies the HOMO of b_g symmetry (Fig. 8). It is noteworthy that the good agreement between the calculated EPR coupling constants based only on the composition of the HOMO and the experimental values confirms that the calculated HOMO is a good function for the unpaired electron.

The electronic spectrum of the radical may be interpreted using full configuration interaction (CI) within the three occupied and one empty (LUMO) molecular orbitals (Fig. 7). The doublet ground-state Ψ_0 is essentially formed by one configuration $(2b_g)^1$ which will be labelled $(^2B_g)_1$. The two next electronic excited terms, relevant for the study of electronic transitions, are Ψ_1 and Ψ_3 based essentially on the mixing of two configurations $(1a_u)^1(2b_g)^2$ and $(2b_g)^0(2a_u)^1$ [eqn. (5)], corresponding to

$$\Psi_1 = (^2A_u)_1 = 0.60\{(1a_u)^1(2b_g)^2\} + 0.77\{(2b_g)^0(2a_u)^1\} + \ldots \quad (5)$$

36% of the first configuration and 60% of the second one [eqn. (6)], corresponding to 53% of the first configuration and

$$\Psi_3 = (^2A_u)_2 = 0.73\{(1a_u)^1(2b_g)^2\} - 0.57\{(2b_g)^0(2a_u)^1\} + \ldots \quad (6)$$

32% of the second one. For the sake of clarity, other less important configurations are omitted in the above expressions.

The Ψ_2 function is still a doublet state, but it belongs to the B_g representation and therefore, the electronic transition $(^2B_g)_1 \longrightarrow (^2B_g)_2$ is orbitally forbidden. The two allowed transitions $\Psi_0 \longrightarrow \Psi_1$ and $\Psi_0 \longrightarrow \Psi_3$ give the calculated excitation energies corresponding to 846 and 496 nm, respectively. These values agree well with the two first low energy bands observed at 806 and 506 nm in the electronic spectrum of $(C_{10}N_8)^{\bullet -}$.

The 806 nm transition is less intense than that at 506 nm. This observation may be explained by an analysis of transition

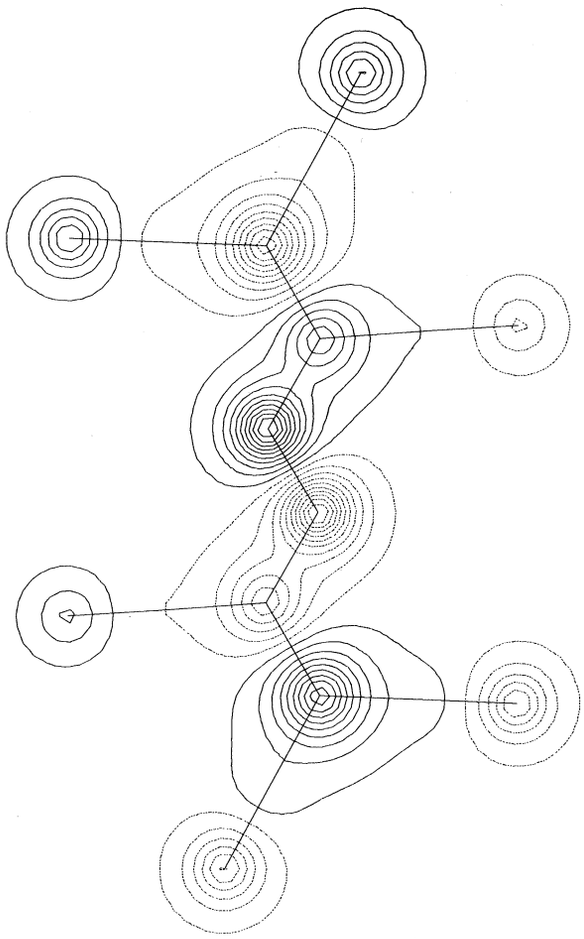

Fig. 8 Plot of the $(C_{10}N_8)^{\bullet -}$ π HOMO orbital. This orbital has a b_g symmetry and is plotted 0.3 Å above the molecular plane.

dipoles involving the above discussed excitations.[25] Let us approximate the Ψ_1 and Ψ_3 by eqns. (7) and (8).

$$\Psi_1 = 2^{-\frac{1}{2}} [\{(1a_u)^1(2b_g)^2\} + \{(2b_g)^0(2a_u)^1\}] \quad (7)$$

$$\Psi_3 = 2^{-\frac{1}{2}} [\{(1a_u)^1(2b_g)^2\} - \{(2b_g)^0(2a_u)^1\}] \quad (8)$$

The transition dipole involving the *x* coordinate (see Fig. 6 for axis definition) for $\Psi_0 \longrightarrow \Psi_1$ is given by eqn. (9), and for the $\Psi_0 \longrightarrow \Psi_3$ transition by eqn. (10).

$$R_{01x} = 2^{-\frac{1}{2}} \left[\int (1a_u)^1(2b_g)^1 x \Psi_0 \, d\tau + \int (2b_g)^0(2a_u)^1 x \Psi_0 \, d\tau \right] \quad (9)$$

$$R_{01x} = 2^{-\frac{1}{2}} [I_{1x} + I_{2x}]$$

$$R_{03x} = 2^{-\frac{1}{2}} [I_{1x} - I_{2x}] \quad (10)$$

The same algebra is valid for *y* and *z* components. Computing the transition dipole components integrals show that eqn. (11) holds, and that $I_{1x} \approx -I_{2x}$.

$$I_{1x} \gg I_{1y}; \quad |I_{2x}| \gg |I_{2y}|; \quad I_{1z} = I_{2z} = 0 \quad (11)$$

This leads to eqn. (12).

$$R_{03} = 2^{-\frac{1}{2}} [I_{1x} - I_{2x}] \gg R_{01} = 2^{-\frac{1}{2}} [I_{1x} + I_{2x}] \quad (12)$$

Since the oscillator strength is proportional to the square of R_{ij}, one concludes that the $\Psi_0 \longrightarrow \Psi_1$ transition should be much less intense than the $\Psi_0 \longrightarrow \Psi_3$ one, in good agreement with the observed spectrum. A similar type of CI effect has been already reported in the electronic spectra of porphyrin systems for which a four orbitals model has been proposed by Gouterman.[25,26] In this last model one weak band labelled as Q and a second strong one (labelled B or Soret) were observed.

The $[(C_{10}N_8)_2]^{2-}$ dimer. In solid state the two radicals $(C_{10}N_8)^{\bullet -}$ stack to form a diamagnetic dimer species $[\{C_{10}N_8)_2]^{2-}$ (Fig. 4). Of course, it is interesting to investigate the change in electronic structures during the dimerization process. This analysis should provide insight into magnetic properties and into the stacking driving force. As for the $(C_{10}N_8)^{\bullet -}$ radical, this study has been performed at the AM1 level of approximation.

Attempts to minimize the geometry of the dimer failed, due to the large electrostatic repulsion between the two negatively charged moieties of the species. In order to relieve this repulsion, we included two cations (NH_4^+ in our model) located at the positions observed for cations in the crystal study. Unfortunately this did not lead to a stable solution: the two negative charges moved to one moiety of the dimer and consequently, the cations migrated towards this doubly charged fragment. Instead of using the crystallographic molecular geometry we preferred to build a more symmetric model by using the structure of the isolated radical $(C_{10}N_8)^{\bullet -}$ previously optimized. The resulting model has a D_2 symmetry and closely fits the X-ray structure.

The binding interaction between two parts of the dimer is strong since the observed interplanar distance of 3.0 Å is short. In order to explain the stability of the dimer, several effects should be taken into account, mainly the electrostatic repulsions, the orbital interactions and the steric hindrances.[27]

Electrostatic interaction should not be neglected since both fragments of the dimer carry a negative charge. However this repulsive effect is balanced by the two cations located at both sides of the dimer.

As shown in the orbital diagram (Fig. 7), the stacking force may be understood in terms of π–π interactions between both radical subsystems. In this diagram, the π orbitals of the monomers $(C_{10}N_8)^{\bullet -}$ belongs to the b_g and a_u representations according to C_{2h} symmetry, the phase and out-of-phase combinations of these orbitals lead to bonding and antibonding functions. The a_g orbitals, which are localized in the constituent monomer planes, represent the lone pairs of the N(1) atoms. They overlap very weakly and consequently do not interact. We used this fact to linearly scale the energy of the dimer to that of the monomers by equalizing the nearly degenerate levels $1b_1$ and 1a of the dimer to that of a_g. The most stabilising effect occurs in the combination of the two singly occupied HOMO $2b_g$ of the monomers leading to the doubly occupied $2b_3$ for the dimer (Fig. 9). As one could expect, the bigger π–π overlap, the greater will be the stabilization energy of the whole system. The best overlap is of course achieved in a perfectly eclipsed conformation which is not the case in $[(C_{10}N_8)_2]^{2-}$. In fact, the overlap requirement is in competition with the steric repulsive effect, thus the overall structure leading to a good orbital overlap and a small steric hindrance should exist. This is well achieved in the dimer since in the actual conformation only four pairs of atoms [N(1) and N(21), N(2) and N(22), C(3) and C(22), C(8) and C(27), Fig. 4] are approximately eclipsed (18 in the eclipsed conformation). The fact that the HOMO electron density of each monomer is essentially located on these atoms (Figs. 8 and 9) leads to a very good overlap while still keeping a low steric repulsive effect.

An interesting optical feature has been reported for such symmetrical or asymmetrical π–π dimers.[28] These systems are formally built by the stacking of two partners with partially filled HOMOs. The HOMO and the LUMO of the dimer are formed by the bonding and the antibonding interactions of two monomer-based HOMOs. This often gives rise to a long-wavelength absorption in the near-infrared (NIR) region of the spectrum. A CI calculation of the singlet excited states for $[(C_{10}N_8)_2]^{2-}$ shows that the singlet ground state is $\{b_3^2\}$ labelled ^1A, while the first excited state, labelled $^1B_1$, is essentially formed in $\{b_3^1 b_2^1\}$ configuration (Fig. 7). The calculated excitation energy for $^1A \longrightarrow {}^1B_1$ transition which is predicted at 1005 nm,

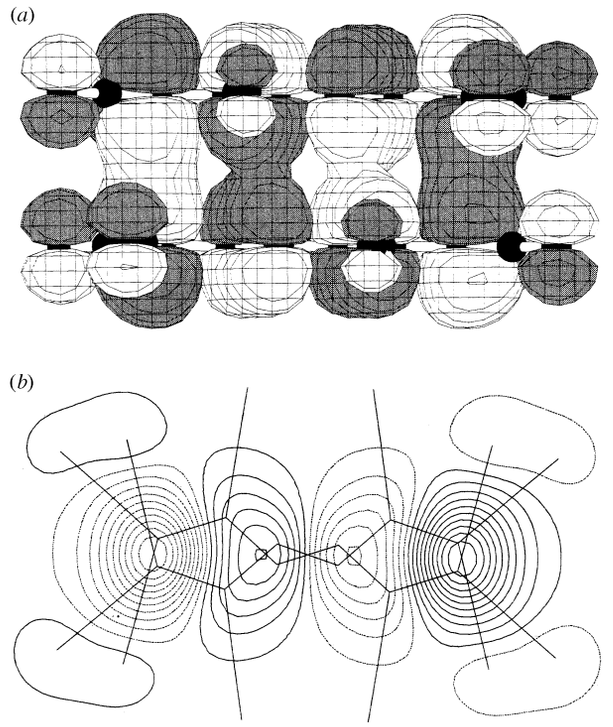

Fig. 9 $[(C_{10}N_8)_2]^{2-}$ π HOMO orbital with b_3 symmetry: top: 3D plot; bottom: plot in the midplane of the dimer

corresponds well to the observed spectrum of $[(C_{10}N_8)_2]^{2-}$ which exhibits a wide absorption band centred at 950 nm. The width of this band is an indication of a large vibronic coupling and the pure electronic transition should so occur at lower energy.[29,30] At this level of approximation (AM1 with the UHF procedure), the triplet state based on the configuration $\{b_3^1b_2^1\}$ exhibits almost the same energy as that of the singlet one. This agrees quite well with the experimental observation consisting of an easy thermal access to the triplet state.

Experimental

IR spectra were obtained with a Perkin-Elmer 1430 spectrometer (KBr pellets). The NIR spectra were recorded on a Varian Cary 5E spectrometer for suspensions in Nujol. EPR spectra were recorded using a JEOL FE 3X spectrometer (X-band). UV–VIS spectra were recorded on a Hewlett Packard 8552 A spectrometer. The apparatus, the three-compartment microelectrochemical cell, the treatment of the solvent and the supporting electrolyte for the electrochemical studies have all been previously described.[31] The reference electrode used is the half-cell: Pt/ferrocenium picrate (10^{-2}), ferrocene (10^{-2}), Bu_4NPF_6 (0.2 M), benzonitrile. For comparison of the present results with other works, the Fc^+/Fc formal potential has been measured *vs.* SCE in benzonitrile (0.2 M Bu_4NPF_6): $E'°(Fc^+/Fc) = +0.43$ V *vs.* SCE.

Tetraethylammonium 1,1,2,5,6,6-hexacyano-3,4-diazahexa-1,5-dienediide 1a and tetraethylammonium 1,1,2,5,6-pentacyano-6-hydrazino-3,4-diazahexa-1,5-dienediide 2a

The literature preparation of Middleton *et al.*[12] was modified as follows. TCNE (6.4 g, 50 mmol) was slowly added at 0 °C to a well-stirred water solution of hydrazine (92 g; 13%). Stirring was maintained for *ca.* 0.5 h; then the mixture was filtered. Solid Et_4NBr (10.5 g, 50 mmol) was added and the resulting precipitate was filtered, dried under vacuum and then extracted with dichloromethane (50 ml). The resulting solution was kept at −20 °C for several hours and then filtered to give **2a** as an orange–red solid (1.5 g, 11%). Addition of diethyl ether to the filtrate afforded **1a** as orange microcrystals (4.9 g, 40%).

The tetrabutylammonium salt **1b** was similarly prepared using Bu_4NBr instead of Et_4NBr. $(Et_4N)_2(C_{10}N_8)$ **1a** (Found: C, 63.4; H, 8.2; N, 28.5. Calc. for $C_{26}H_{40}N_{10}$: C, 63.4; H, 8.2; N, 28.4%). $\lambda_{max}(CH_3CN)$/nm 474 and 454. ν_{max}/cm^{-1} 2220w, 2170s, 2140s and 2120sh (ν_{CN}). δ_H[300 MHz, $(CD_3)_2SO$, $SiMe_4$] 1.30 (12 H, m, CH_3), 3.45 (8 H, m, CH_2). δ_C[300 MHz, $(CD_3)_2SO$, $SiMe_4$]: 36.6 [s, *C*(CN)], 112.1 [s, CC(*CN*)$_2$], 120.8 (s, C*CN*), 135.5 [s, C*C*(CN)$_2$].

$(Et_4N)_2(C_9N_9H_3)$, 1.5 H_2O **2a** (Found: C, 57.6; H, 8.2; N, 30.3. Calc. for $C_{25}H_{43}N_{11}$, 1.5 H_2O: C, 57.2; H, 8.8; N, 29.4%). ν_{max}/cm^{-1} 2220w, 2180s, 2150s and 2120sh (ν_{CN}); 3360w and 3200w (ν_{NH}). δ_H[300 MHz, $(CD_3)_2SO$, $SiMe_4$]: 1.30 (24 H, m, CH_3), 3.45 (16 H, m, CH_2), 4.95 (1 H, NH), 6.10 (2 H, NH_2). δ_C[300 MHz, $(CD_3)_2SO$, $SiMe_4$]: 29.6 and 75.2 [s, *C*(CN)], 110.0, 116.8, 122.7, 122.9, 123.8 (s, CN), 159.5 [s, *C*(CN)$_2$]. CV (PhCN): 4 irr. oxid. pks at −0.36, −0.14, +0.11 and +0.90 V (ref. Fc^+/Fc).

Tetraethylammonium 1,1,2,5,6,6-hexacyano-3,4-diazahexa-1,5-dieneide 3a

The synthesis was performed in Schlenk tubes under dry oxygen-free nitrogen. To a dichloromethane solution of **1a** (0.25 g, 0.5 mmol) was slowly added with stirring a dichloromethane solution (25 ml) of iodine (0.25 g, 1 mmol). The resulting dark precipitate which appeared was filtered, washed with diethyl ether and dried *in vacuo* (0.14 g, 80%) (Found: C, 58.9; H, 5.6; N, 34.5. Calc. for $C_{18}H_{20}N_9$: C, 59.6; H, 5.6; N, 34.8%). $\lambda_{max}(CH_3CN)$/nm 806, 506 and 476. ν_{max}/cm^{-1} 2200s (ν_{CN}). EPR (powder, room temp.): $g_{xx} = 2.004$; $g_{yy} = 2.003$; $g_{zz} = 2.002$; $|D|/hc = 0.0126$ cm^{-1}; $|E|/hc = 0.0020$ cm^{-1}.

X-Ray structure analysis

Orange crystals of $(Bu_4N)_2(C_{10}N_8)$ **1b** were obtained from a dichloromethane–diethyl ether solution which was allowed to stand at −20 °C; dark crystals of $(Et_4N)(C_{10}N_8)$ **3a** were similarly obtained from an acetone–diethyl ether solution. Intensity data were collected on an Enraf–Nonius CAD 4 X-ray diffractometer with graphite-monochromated Mo-Kα ($\lambda = 0.710\,73$ Å) using the ω–2θ scan technique; a summary of the crystallographic data is reported in Table 2. Cell parameters of both compounds were determined by least-squares refinement of diffractometer setting angles for 25 carefully centred reflections. The intensities of three standard reflections were monitored periodically during data collection. There was no significant decay (<0.4%) during any of the data collections. Intensity data were corrected for Lorentz and polarization effects, the structures were solved with direct methods which reveal all non-hydrogen atoms.§

$(Bu_4N)_2(C_{10}N)$ **1b**. All the hydrogen atoms were found with a Fourier difference between 0.41 and 0.23 e Å^{-3} and refined with an isotropic thermal parameter *B* of 4 Å^2. Anisotropic thermal parameters were used with all the non-hydrogen atoms.

$(Et_4N)(C_{10}N_8)$ **3a**. The structure was refined in two parts since the number of observed reflections was low (small sample). The non-hydrogen atoms were refined with anisotropic thermal parameters, except for all carbon atoms of the cations. Some of the later showed high thermal motion and disorder; in particular, two CH_2 carbon atoms of a cation were located in two sites with occupancy factors of 0.5. All the hydrogen atoms were introduced in calculated positions, with an overall temperature factor of 6 Å^2 in the final cycle of refinement. All calculations, carried out on a Digital MicroVAX 3100 computer, were performed using the MOLEN set of programs.[32] Atomic scatter-

§ Atomic coordinates, bond lengths and angles, and thermal parameters have been deposited at the Cambridge Crystallographic Data Centre (CCDC). For details of the deposition scheme, see 'Instructions for Authors', *J. Chem. Soc., Perkin Trans. 2*, 1997, Issue 1. Any request to the CCDC for this material should quote the full literature citation and the reference number 188/47.

Table 2 Crystal and refinement data for $(Bu_4N)_2(C_{10}N_8)$ **1b** and for $(Et_4N)(C_{10}N_8)$ **3a**

Formula	$C_{42}H_{72}N_{10}$ **1b**	$C_{18}H_{20}N_9$ **3a**
Molecular mass	717.1	362.4
Crystal system	triclinic	monoclinic
Space group	$P\bar{1}$	Cc
a/Å	9.841(2)	25.124(9)
b/Å	10.126(3)	12.855(4)
c/Å	12.995(2)	12.36(2)
α/°	110.25(2)	
β/°	100.87(2)	95.07(6)
γ/°	101.24(2)	
V/Å^3	1144	3976
Z	1	8
ρ_{calc} (g cm^{-3})	1.04	1.21
$F(000)$	394	1528
μ(Mo-Kα)/cm^{-1}	0.59	0.74
T/K	294	294
Crystal size/mm	0.30 × 0.50 × 0.60	0.08 × 0.10 × 0.50
Radiation	Mo-Kα	Mo-Kα
Max 2θ/°	50	50
Scan	$\omega/2\theta = 1$	$\omega/2\theta = 1$
Variance of standards	0.3%	0.4%
Range of hkl	0,12; −12,12; −16,16	−29,29; 0,15; 0,14
Reflections measured	4763	3858
Reflections observed [$I > n\sigma(I)$]	2539 ($n = 4$)	1159 ($n = 1.5$)
R_{int} (from merging equiv refl)	0.009	0.024
N(obs)/N(var)	2539/344	1159/245
R [a]	0.051	0.075
R_w [b]	0.045	0.070
Max residual/e Å^{-3}	0.18	0.13
Goodness of fit [c]	0.74	2.00
Δ/σ	0.12	0.03

[a] $R = \Sigma[||F_o| - |F_c||]/\Sigma|F_o|$. [b] $R_w = [\Sigma w(|F_o| - |F_c|)^2/\Sigma w|F_o|^2]^{\frac{1}{2}}$; $w = 4F_o^2/[\sigma^2(|I|) + (0.04|F_o|^2)^2]$. [c] Goodness of fit (GOF) = $[\Sigma w(|F_o| - |F_c|)^2/(N_{obs} - N_{var})]^{\frac{1}{2}}$.

ing factors were taken from International Tables for X-Ray Crystallography.[33]

Acknowledgements

We wish to express our gratitude to Professor J. E. Guerchais (Brest) for fruitful discussions and helpful advice and to Professor D. Grandjean (Rennes) for calculation facilities. We greatly appreciate the assistance supplied by Dr S. Triki and J. M. Kerbaol (Brest) as well as the magnetic susceptibility data taken by Dr P. Molinié and Dr A. Leblanc (Institut des Matériaux, Nantes). This work was supported by a fellowship (M. D.) from Région Bretagne for which we are grateful.

References

1 A. J. Fatiadi, *The Chemistry of Triple Bonded Groups*, Wiley, New York, 1983; *Synthesis*, 1986, 249; 1987, 749; 1987, 959.
2 W. Kaim and M. Moscherosch, *Coord. Chem. Rev.*, 1994, **129**, 157.
3 W. E. Buschmann, A. M. Arif and J. S. Miller, *J. Chem. Soc., Chem. Commun*, 1995, 2343.
4 A. Aumüller, P. Erk, G. Klebe, S. Hünig, J. U. von Schütz and H. P. Werner, *Angew. Chem., Int. Ed. Engl.*, 1986, **25**, 740.
5 H. Yamochi, S. Horiuchi, G. Saito, M. Kusonoki, K. Sakaguchi, T. Kikuchi and S. Sato, *Synth. Met.*, 1993, **56**, 2096.
6 T. Sugimoto, M. Tsujii, E. Murahashi, H. Nakatsuji, J. Yamauchi, H. Fujita, Y. Kai and N. Hosoito, *Mol. Cryst. Liq. Cryst.*, 1993, **232A**, 117.
7 W. J. Middleton, USP 2 762 811/1956; *Chem. Abstr.*, 1956, **51**, 4722.
8 M. Bonamico, V. Fares, A. Flamini, A. M. Giuliani and P. Imperatori, *J. Chem. Soc., Perkin Trans. 2*, 1988, 1447.
9 J. E. Lind, Jr., and R. M. Fuoss, *J. Am. Chem. Soc.*, 1961, **83**, 1828.
10 A. L. Farragher and F. M. Page, *Trans. Faraday Soc.*, 1967, **63**, 10.
11 M. L. Bruce, R. C. Wallis, B. W. Skelton and A. H. White, *J. Chem. Soc., Dalton Trans.*, 1981, 1205.
12 W. J. Middleton, E. L. Little, D. D. Coffman and A. V. Engelhardt, *J. Am. Chem. Soc.*, 1958, **80**, 2795.
13 M. Decoster, J. E. Guerchais, Y. Le Mest, J. Sala Pala, S. Triki and L. Toupet, *Polyhedron*, 1996, **15**, 195.
14 C. Vazquez, J. C. Calabrese, D. A. Dixon and J. S. Miller, *J. Org. Chem.*, 1993, **58**, 65.
15 F. M. Allen, O. Kennard, D. G. Watson, L. Bramer, A. J. Orpen and R. Taylor, *J. Chem. Soc., Perkin Trans. 2*, 1987, S1.
16 J. J. Mayerle, *Mixed-valence Compounds*, ed. D. B. Brown, Reidel, New York, 1980, p. 461.
17 A. Bencini and C. Zanchini, *Inorg. Chem.*, 1991, **30**, 4245.
18 D. O'Hare, M. D. Ward and J. S. Miller, *Chem. Mater.*, 1990, **2**, 758.
19 E. Wasserman, L. C. Snyder and W. A. Yager, *J. Chem. Phys.*, 1964, **41**, 1763.
20 J. S. Miller, P. J. Krusic, D. A. Dixon, W. M. Reiff, J. H. Zhang, E. C. Anderson and A. J. Epstein, *J. Am. Chem. Soc.*, 1986, **108**, 4459.
21 J. S. Miller, D. A. Dixon, J. C. Calabrese, C. Vazquez, P. J. Krusic, M. D. Ward, E. Wasserman and R. L. Harlow, *J. Am. Chem. Soc.*, 1990, **112**, 381.
22 J. S. Miller, M. D. Ward, J. H. Zhang and W. M. Reiff, *Inorg. Chem.*, 1990, **29**, 4063.
23 F. E. Mabbs and D. Collison, *Studies in Inorganic Chemistry, Vol. 16: Electron Paramagnetic Resonance of d Transition Metal Compounds*, Elsevier, Amsterdam, 1992.
24 M. J. S. Dewar, E. G. Zoebisch, E. F. Healy and J. J. P. Stewart, *J. Am. Chem. Soc.*, 1985, **107**, 3902.
25 F. Adar, *The Porphyrins*, ed. D. Dolphin, Academic Press, New York, 1978, vol. 3, p 172.
26 M. Gouterman, *J. Mol. Spectrosc.*, 1961, **6**, 138.
27 T. J. Marks, *Angew. Chem., Int. Ed. Engl.*, 1990, **29**, 857.
28 J. K. Duchowski and D. F. Bocian, *J. Am. Chem. Soc.*, 1990, **112**, 3312.
29 R. J. Donohoe, J. K. Duchowski and D. F. Bocian, *J. Am. Chem. Soc.*, 1988, **110**, 6119.
30 S. B. Piepho, *J. Am. Chem. Soc.*, 1988, **110**, 6319.
31 Y. Le Mest, M. L'Her, N. H. Hendricks, K. Kim and J. P. Collman, *Inorg. Chem.*, 1992, **31**, 835.
32 C. K. Fair, MOLEN, *An Interactive Intelligent System for Crystal Structure Analysis*, Enraf–Nonius, Delft, The Netherlands, 1990.
33 *International Tables for X-ray Crystallography*, vol. IV, Kynoch Press, Birmingham, 1974.

Paper 6/05243F
Received 26*th July* 1996
Accepted 10*th October* 1996